INFORMATICS JOURNALS

Research Article

Journal of Natural Remedies
DOI: 10.18311/jnr/2026/49467

eISSN: 2320-3358 | Vol 26(1), 2026 | pp. 99-120

Exploring the Anti-diabetic Potential of *Sida cordata*: An *In Silico* Study through Molecular Docking and Dynamics Simulation

Mahesh Kumar[1], Sangeetha Mani[1*], Ethayaraja Mani[2] and Alan M. Punnoose[3]

[1]Sri Ramachandra Faculty of Pharmacy, Sri Ramachandra Institute of Higher Education and Research (DU), Porur, Chennai - 600116, Tamil Nadu, India; maheshkumars@sriramachandra.edu.in

[2]Department of Chemical Engineering, IIT Madras, Chennai - 600036, Tamil Nadu, India

[3]Sri Ramachandra Faculty of Clinical Research, Stem Cell Regenerative Biology Lab, Sri Ramachandra Institute of Higher Education and Research (DU), Porur, Chennai - 600116, Tamil Nadu, India

Abstract

Background: Diabetes mellitus is a progressive metabolic disorder characterise by chronic hyperglycemia and impaired carbohydrate metabolism. Despite the availability of synthetic antidiabetic agents, their long-term administration is often associated with adverse effects, which stresses the urgent need for safer alternatives of plant origin. *Sida cordata* is a traditionally valued medicinal plant reported to exhibit antidiabetic and organ-protective actions; however, its detailed molecular mechanism for antidiabetic activity is not yet well established. **Aim:** To explore in depth, through in silico molecular docking and molecular dynamics simulations, the potential mechanisms of *S. cordata* phytoconstituents as an antidiabetic agent against important protein targets associated with diabetes. **Methods:** Twenty-eight *S. cordata* phytoconstituents were screened against four diabetes-related proteins (PDB IDs: 7VSI, 7WMV, 4EMA and 1KAV) using Schrödinger Glide for molecular docking. The stability and dynamic behavior of the top-scoring protein-ligand complexes were further investigated by molecular dynamics simulations conducted with GROMACS.ADMET and drug-likeness were predicted using SwissADME to assess pharmacokinetics. **Results:** The molecular docking analysis of all screened phytoconstituents revealed favorable binding affinities as evidenced by the obtained docking scores ranging from -1.4 to -12.9 kcal/mol. Notably, α-D-glucopyranoside, O-α-D-glucopyranosyl-(1→3)-α-D-fructofuranosyl exhibited the highest and most consistent binding to all targets, reaching a maximum docking score of -12.9 kcal/mol against 7VSI. Thus, an interaction analysis was conducted, which revealed stable hydrogen bonding and hydrophobic interactions within the active site. Molecular dynamics simulations demonstrated structural stability for both 7VSI-lead compound and 7VSI-standard complexes, with the least root-mean-square deviation for the entire period of the simulation study. The ADMET analysis revealed that the selected lead compound exhibited acceptable pharmacokinetic properties, good oral bioavailability, and no predicted toxicity. These findings support its drug-likeness and suitability for further antidiabetic development. The current findings support the antidiabetic potential of *S. cordata*, in particular its α-D-glucopyranoside derivatives, through *in silico* results indicating high binding affinities and biologically stable protein-ligand interactions with target proteins associated with diabetes.

Major Findings: *Sida cordata* phytoconstituents demonstrated strong and consistent binding to multiple diabetes-related protein targets. The α-D-glucopyranoside derivative emerged as a stable lead compound, validated through molecular docking and dynamics simulations.

Keywords: α-D-glucopyranoside, Diabetes Mellitus, Dynamics Stimulation, GC-MS, Molecular Docking, *Sida cordata*, Traditional Medicine

(Article Chronicle: Article Received on: 17.04.2025; Revised on: 30.12.2025; Accepted on: 12.01.2026)

*Author for correspondence

1. Introduction

A chronic metabolic disorder, Diabetes Mellitus (DM) is characterised by the presence of hyperglycemia, a condition marked by abnormally high blood sugar levels. This metabolic dysregulation arises from defects in insulin secretion, insulin action, or both. With a staggering global prevalence exceeding 422 million people, DM represents a significant healthcare burden, posing a major threat to global health[1]. While conventional therapies exist for managing diabetes, there is a growing interest in exploring complementary and alternative treatment options, particularly those utilizing herbal medicines. Numerous plants have been used traditionally for centuries to manage diabetes, offering a wealth of potential for discovering novel therapeutic agents[2]. The exploration of these natural products with antidiabetic properties holds promise for the development of new and potentially more holistic treatment strategies[3].

Sida cordata (Burm.f.) Bross. waalk. (Family: *Malvaceae*), also known as "*bala*" or "flannel bush," is a small herbaceous plant indigenous to Asia. It has a long history of use in traditional Ayurvedic medicine for treating various ailments, including diabetes mellitus, asthma, inflammation, wound healing, and skin disorders. This widespread ethnomedicinal use positions *S. cordata* as a promising candidate for antidiabetic investigation. *S. cordata* is rich in various phytochemicals, including flavonoids, alkaloids, and polyphenols[4]. These bioactive constituents present in the whole plant are considered key contributors to its pharmacological potential. Their synergistic actions are likely responsible for the observed therapeutic and health benefits.

In silico methods, particularly molecular docking and dynamics simulations, have emerged as powerful tools for investigating the interaction between potential drugs and their targets at the molecular level[5]. Protein structures offer insights into diabetes medications and effective treatments for diabetes. Two protein structures deposited in the RCSB Protein Data Bank (PDB) provide valuable information on how different medications work. The structure (PDB ID: 4EMA) details the interaction between Rosiglitazone, a medication for type 2 diabetes, and PPARγ, a protein regulating glucose metabolism[6]. Understanding this interaction at the atomic level allows researchers to design new drugs targeting this pathway for better diabetes management[7]. The structure (PDB ID: 7VSI) focuses on a complex involving SGLT2 (a protein responsible for reabsorbing glucose in the kidneys), MAP17 (a protein interacting with SGLT2), and Empagliflozin (an SGLT2 inhibitor medication). This structure reveals how Empagliflozin binds to SGLT2, locking it in an open conformation that prevents glucose reabsorption and lowers blood sugar. This knowledge can be used to develop improved SGLT2 inhibitors. These protein structures (including 7WMV, which offers insights into a potential SGLT1 inhibitor) are instrumental for researchers developing more effective diabetes treatments by targeting different molecular mechanisms[8]. 1KAV structure reveals human PTP1B bound to inhibitors, providing insights for drug design. The structure identifies the binding pocket and suggests potential for dual binding, but selectivity remains a challenge. This information paves the way for more potent and specific PTP1B inhibitors for diabetes treatment[9].

This approach offers several advantages over traditional experimental methods, particularly in the early stages of drug discovery[10]. Rapid Screening Docking simulations can rapidly screen a large number of bioactive compounds present in the whole plant part of *S. cordata* extract, allowing researchers to identify those with the most promising binding affinities for relevant diabetic targets, such as enzymes involved in glucose metabolism. Dynamic insights following up on promising docking results, molecular dynamics simulations provide a more dynamic picture of ligand-receptor interactions. These simulations reveal the stability and nature of the complex over time, offering valuable insights into the potential mechanisms of action[11].

Current diabetes drugs are effective, but can cause side effects. Plant extracts offer a natural approach, but lack strong scientific backing. Combining both might be the best proven control with potentially fewer side effects[12]. This research paper delves into the antidiabetic potential of *S. cordata* extract through a combined approach of *in silico* docking and dynamics simulations. We will focus on the interaction between the identified bioactive compounds in the extract and key enzymes involved in glucose metabolism, such as alpha-amylase, alpha-glucosidase, and PPARγ[13]. These enzymes play

crucial roles in carbohydrate digestion and cellular insulin sensitivity. By utilising these computational techniques, we aim to identify the bioactive compounds in *S. cordata* extract with the most promising binding affinities for these key diabetic targets. Gain insights into the mechanisms by which *S. cordata* extract may exert its antidiabetic effects through detailed analysis of the ligand-receptor interactions. The results of this research will enhance current knowledge on the role of herbal remedies in diabetic management and guide further *in vitro* and *in vivo* investigations to validate these *in silico* predictions. Exploring the antidiabetic potential of *S. cordata* holds significant promise for the development of novel therapeutic strategies. This research leverages *in silico* methods to bridge the gap between traditional knowledge and scientific understanding. Through this combined approach of docking and dynamics simulations, we aim to elucidate the mechanisms by which *S. cordata* extract may influence glucose metabolism and pave the way for further research into this promising herbal remedy for diabetes management[14].

2. Materials and Methods

2.1 Collection of Compounds

GC–MS analysis of *S. cordata* reported a total of 38 phytoconstituents. However, only 28 compounds were selected for molecular docking based on the availability of complete and well-defined chemical structures, structural suitability for *in silico* analysis, and potential biological relevance. Compounds with simple aliphatic hydrocarbons with limited relevance to enzyme inhibition were excluded to ensure computational accuracy and meaningful interpretation of the docking results. *S. cordata* contains diverse phytochemical constituents, including alkaloids, flavonoids, phenolic compounds, glycosides, tannins, terpenoids, fatty acids, and sterols, which contribute collectively to its pharmacological activities[15] (Table 1).

2.2 Molecular Docking

2.1.1 Preparation of the Protein

In molecular docking, different proteins related to diabetes were targeted. The PDB ID of proteins are 7VSI- Structure of human SGLT2-MAP17 complex bound with Empagliflozin, 7WMV- Structure of human SGLT1-MAP17 complex bound with LX2761, 4EMA- Human peroxisome proliferator-activated receptor gamma in complex with Rosiglitazone, 1KAV - Human Tyrosine Phosphatase 1B Complexed with an Inhibitor; these proteins were obtained from Protein Data Bank.

Protein preparation was performed using the Protein Preparation Wizard of Schrodinger Suite (Version 2023-2). Missing hydrogen atoms were added, bond orders were assigned, and water molecules beyond 5 Å from hetero groups were removed. The protein structures were optimised and minimised using the OPLS4 force field to relieve steric clashes and obtain stable conformations for docking studies. It is the primary crystallographic database designed to provide 3D structural information about big molecules like nucleic acids and proteins. Once NMR and X-ray crystallography were completed, the structures were created. After extracting all of the proteins from the Protein Data Bank (https://www.rcsb.org/), polar hydrogen was added to each protein in preparation for the molecular docking procedure[16].

2.1.2 Preparation and Optimisation of the Ligand

A total of twenty-eight phytoconstituents of *S. cordata* were selected for *in silico* studies based on GC–MS analysis and supporting phytochemical literature. The two-dimensional (2D) chemical structures of the selected compounds were retrieved from the PubChem database. For compounds lacking complete structural information, molecular structures were manually drawn using ChemDraw Professional 20.0 and verified. All ligand structures were initially sketched and optimised using ChemSketch, and the resulting files were saved in MOL2 format[17].

Ligand structures were initially optimised by removing associated water molecules, adding missing hydrogen atoms, and assigning appropriate partial charges. Gasteiger charges were applied to non-standard residues, while parameters for standard residues were assigned using the AMBER ff14SB force field, where applicable. The optimised ligands were then imported into UCSF Chimaera and converted into three-dimensional (3D) conformations. Final ligand preparation was carried out using the LigPrep module (Schrodinger Suite) to generate energetically minimised 3D structures, assign appropriate protonation states at

Table 1. Phytoconstituents of *S. cordata*

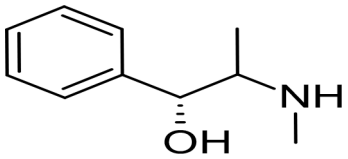
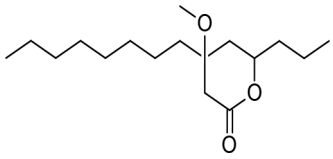
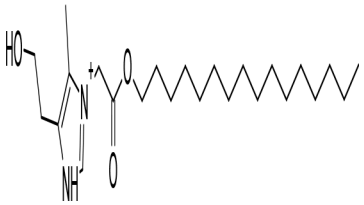
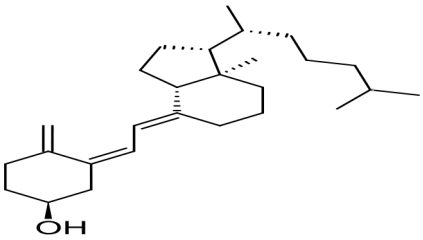
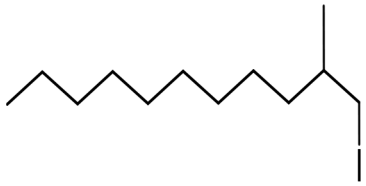
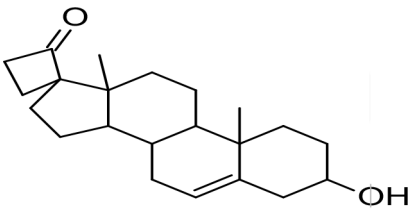
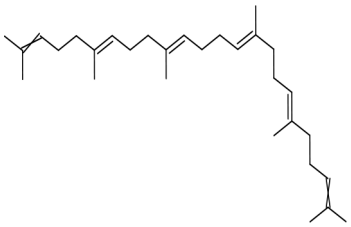
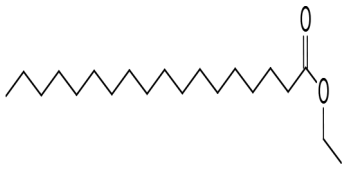
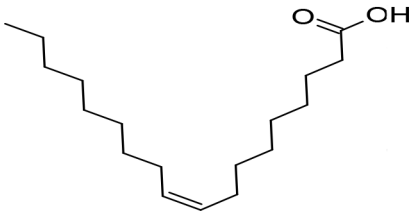
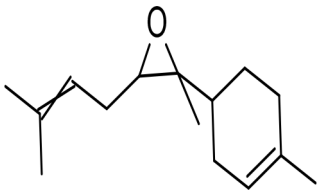
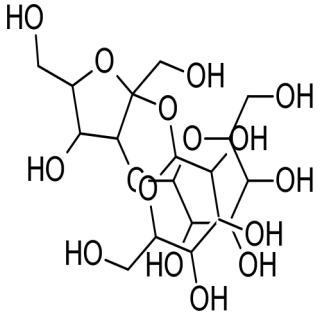
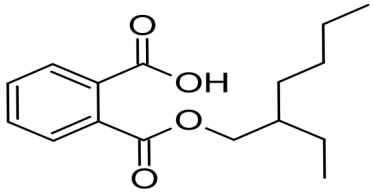
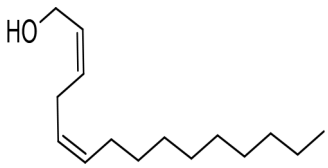
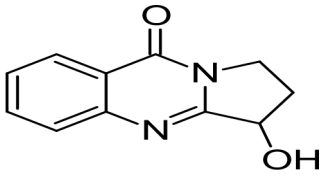
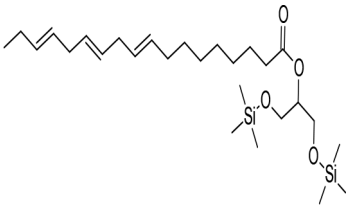
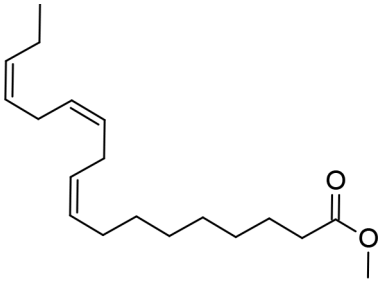
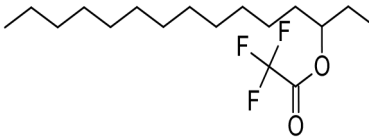
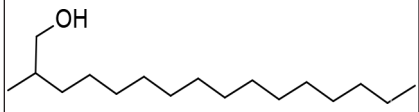
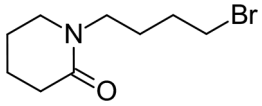
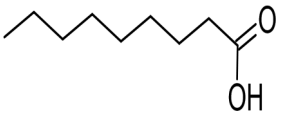
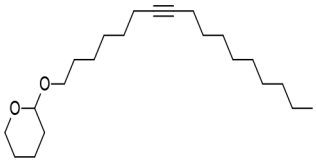
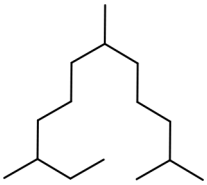
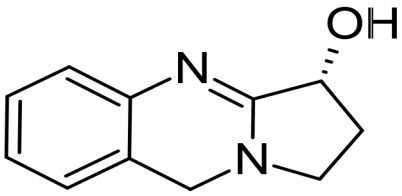
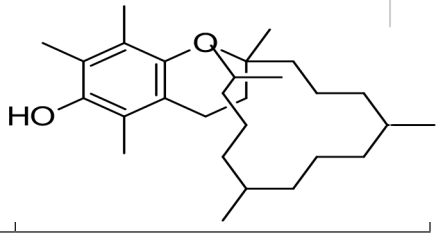
Compound name	Structure	Compound name	Structure
1-2-Methylamine-1-phenyl propanol		Methoxy acetic acid, 4-tetradecyl ester	
2-Hexade cycloxycarbonyl-5-(2-hydroxyethyl)-4-methylimidazolium ion		1,2-15,16-Diepoxyhexadecane	
Vitamin D_3		1-iodo-2-methylundecane	
Spiro[androst-5ene-17,1-Cyclobutane]-2-one,3-hydroxy-, (3a,17a)-		Squalene	
Octadecanoic acid, ethyl ester		Oleic acid	
Cis-Z-a-Bisbolene epoxide		a-D-glucopyranoside,O-a-D-glucopyranosyl-(1.fwdard.3)-a-D-fructofuranosyl	
Diethylene glycol monododecyl ether		1,2-Benezene dicarboxylic acid, mono(2-ethylhexyl) ester	

Table 1. Continued...

Compound name	Structure	Compound name	Structure
Z,Z-2,5-pentadecadien-1-ol		3S-Hydroxy-2,3-dihydro-1H-pyrrolo [2,1-b] quinazolin-9-one	
Octadecane, 1-(ethenyloxy)-		9,12-octadecadienoic acid, methyl ester, (E,E)	
9,12,15-octadecatrienoic acid,2-[(trimethylsilyl)oxy]-1-[[trimethylsilyl) oxy]methyl] ethyl ester (Z,Z,Z)		9,12,15-octadecadienoic acid,methyl ester, (Z,Z,Z)	
3-Trifluroa cetoxypentadecane		1-Hexadecanol, 2-methyl-	
2-piperidinone, N-[4-bromo-n-butyl]		Nonanoic acid	
2H-pyran,2-(7-heptadecynyloxy) tetrahydro-		Dodecane, 2,6,10-Trimethyl-	
[3R]-1,2,3,9-tetrahydropyrrolo [2,1-b] quinazolin-3-ol		Vitamin E	

physiological pH (7.0 ± 0.2), and generate relevant stereoisomers. This standardised ligand preparation protocol ensured structural accuracy, consistency, and suitability for subsequent molecular docking and molecular dynamics simulations[18].

2.1.3 Molecular Docking Using Schrodinger

Molecular docking studies were performed using the crystal structures of selected diabetes-related target proteins. The docking workflow was executed using Schrodinger Suite, with visualization and interaction

analysis supported by UCSF Chimaera and Discovery Studio 4.1. Protein structures were pre-processed by removing water molecules, adding hydrogen atoms, and optimizing bond orders to obtain stable conformations suitable for docking analysis.

A total of 38 phytoconstituents were identified from the GC–MS analysis of *S. cordata*. Among these, **28 compounds** were selected for molecular docking based on the availability of well-defined chemical structures, completeness of molecular information, and suitability for *in silico* enzyme-inhibition studies. Compounds lacking definitive structural data, exhibiting highly fragmented mass spectra, or representing long-chain aliphatic hydrocarbons with limited relevance to protein–ligand interactions were excluded to ensure computational reliability and biological relevance.

The two-dimensional structures of the selected phytoconstituents were retrieved from the PubChem database and drawn using ChemDraw Professional 20.0, where required. Ligand preparation was carried out using LigPrep (Schrodinger Suite) to generate energetically minimised three-dimensional conformations, assign appropriate protonation states at physiological pH (7.0 ± 0.2), and generate relevant stereoisomers.

Prepared ligands were subsequently converted into PDBQT format, and all rotatable bonds were made flexible to enable effective conformational sampling during docking. The docking grid was generated by centring it on the active site of the target protein, with a grid box dimension of 75 × 75 × 75 Å along the x, y, and z axes to ensure complete coverage of the binding pocket. Docking was performed individually for each ligand, and binding affinities were calculated in kcal/mol. Post-docking interaction analysis was conducted using Discovery Studio 4.1 to examine hydrogen bonding, hydrophobic interactions, and key amino acid residues involved in ligand binding. This systematic ligand selection and docking strategy ensured structural accuracy, reproducibility, and meaningful interpretation of the molecular interactions underlying the antidiabetic potential of *S. cordata* phytoconstituents.

2.3 Molecular Dynamics

2.3.1 Molecular Dynamics Simulation

Molecular dynamics (MD) simulations were performed to evaluate the conformational stability and dynamic behaviour of the top-ranked protein–ligand complexes identified from molecular docking studies. The compound exhibiting the highest binding affinity, α-D-glucopyranoside, was selected for MD analysis and compared with the apo protein (7VSI-APO) and a standard drug complex (7VSI-STD; empagliflozin). Accordingly, three systems—7VSI-APO, 7VSI-DRG (α-D-glucopyranoside), and 7VSI-STD—were subjected to molecular dynamics simulations.

All simulations were carried out using GROMACS version 2022.3 with the CHARMM36 force field. Ligand topology and parameter files were generated using the CHARMM General Force Field (CGenFF) server. Each system was solvated in a triclinic box containing TIP3P water molecules and neutralised by adding appropriate counter-ions. Energy minimisation was performed using the steepest descent algorithm to remove steric clashes and optimise system geometry. Following minimisation, equilibration was conducted in two phases: constant volume and temperature (NVT) for temperature stabilisation, followed by constant pressure and temperature (NPT) to equilibrate system density. Both equilibration phases were performed for 100 ps at 300 K using the V-rescale thermostat and Parrinello–Rahman barostat. After equilibration, production MD simulations were carried out for 200 ns for each system under periodic boundary conditions.

Structural stability and conformational changes during the simulation were evaluated using Root Mean Square Deviation (RMSD) and radius of gyration (Rg) analyses. RMSD was used to assess deviations of the protein backbone over time, while Rg provided insights into the compactness and folding stability of the protein structures. Additionally, hydrogen bond analysis between the protein and ligands was performed throughout the simulation to evaluate the persistence and strength of intermolecular interactions, serving as an indicator of complex stability. The data were saved at regular intervals for detailed post-simulation analysis, and final structures were extracted for visualisation and interaction mapping. The combined MD results provided dynamic validation of docking outcomes and confirmed the sustained stability of the protein–ligand complexes under physiological conditions.

2.4 ADMET and Drug-likeness Analysis

The pharmacokinetic properties and drug-likeness of the top-performing phytoconstituents were evaluated using the SwissADME web server. Parameters including Lipinski's rule of five, gastrointestinal absorption, blood–brain barrier permeability, cytochrome P450 inhibition, and toxicity alerts were analysed to assess the suitability of compounds as oral antidiabetic agents.

3. Results

On the basis of the GC-MS report, the total 28 constituents of the plant *S. cordata* were docked with the anti-diabetic proteins and the images are mentioned in the supplementary report.

3.1 Molecular Docking Analysis

Molecular docking was performed to evaluate the binding affinity of 28 phytoconstituents of *S. cordata* against four diabetes-associated target proteins (PDB IDs: 7VSI, 4EMA, 7WMV, and 1KAV. The docking scores obtained from Glide XP ranged from −1.27 to −12.95 kcal/mol, indicating variable but target-specific binding efficiencies (Table 1). Among all tested compounds, α-D-glucopyranoside, O-α-D-glucopyranosyl-(1→3)-α-D-fructofuranosyl exhibited the highest binding affinity toward all four targets, with docking scores of (Figure 1A) −12.945 (7VSI), (Figure 3 A) −11.231 (4EMA), (Figure 2 A) −10.961 (7WMV), and (Figure 4 A) −7.522 kcal/mol (1KAV). The significantly lower docking scores suggest a strong and stable interaction within the catalytic pockets of these enzymes, highlighting this compound as the most promising antidiabetic lead molecule in the present study. Several other compounds, including (Figure 1C) 3-trifluoroacetoxypentadecane, (Figure 3, D) 2-piperidinone, N-[4-bromo-n-butyl], and (Figure 2D) 1,2-benzenedicarboxylic acid mono(2-ethylhexyl) ester, also demonstrated moderate to strong binding affinities, particularly against 4EMA and 7WMV, indicating possible multi-target inhibitory potential. (Table 2).

3.2 Protein–ligand Interaction Analysis

A detailed interaction analysis revealed that the bioactive compounds were stabilized within the binding pockets predominantly through hydrophobic interactions, along with hydrogen bonding and van der Waals forces, which are critical for enzymatic inhibition. The active site of 7VSI is primarily composed of hydrophobic residues such as LEU353, PHE303, MET364, MET318, LEU320, PHE297, CYS285, ILE249, LEU255, ILE341, and VAL339 (Figure 1A-F). The top-ranked compound, α-D-glucopyranoside derivative, formed multiple hydrogen bonds with CYS285 and PHE297, while being deeply stabilised by hydrophobic contacts with LEU353, MET364, and ILE341. These interactions strongly support its inhibitory potential by anchoring the ligand firmly within the catalytic cavity. (Table 3). Docking against 7WMV revealed that residues such as LEU453, LEU465, PHE363, MET364, LEU469, TYR473, ALA292, ILE326, TRP327, and MET334 played a crucial role in ligand recognition (Figure 2 A-F). The α-D-glucopyranoside derivative showed consistent hydrogen bonding with ALA292 and TYR473, along with strong hydrophobic stabilization via LEU453, MET334, and PHE363, suggesting effective inhibition of enzymatic activity (Table 4). In the case of 4EMA, key interacting residues included TYR473, LEU469, MET348, PHE282, ILE281, CYS285, PHE363, and MET364. The selected lead compound exhibited hydrogen bond interactions with TYR473 and CYS285, while extensive hydrophobic interactions with LEU469, MET364, and PHE363 contributed to binding stability. (Figure 3 A-F) TYR473 is a well-known regulatory residue in glucose-metabolizing enzymes, indicating functional relevance of the interaction (Table 5). For 1KAV, binding was dominated by interactions with LEU255, MET318, ILE341, LEU340, VAL339, TRP327, MET334, LEU353, and TYR473. (Figure 4 A-B) The lead compound established hydrogen bonding with TYR473 and hydrophobic interactions with LEU340, MET334, and ILE341, indicating a stable ligand–protein complex. (Table 6).

3.3 Molecular Dynamics

High-resolution Molecular Dynamics (MD) simulation is an effective tool for exploring the structural dynamics of proteins and their interactions with bioactive compounds. This method has transformed the landscape of Computer-aided Drug Design (CADD)

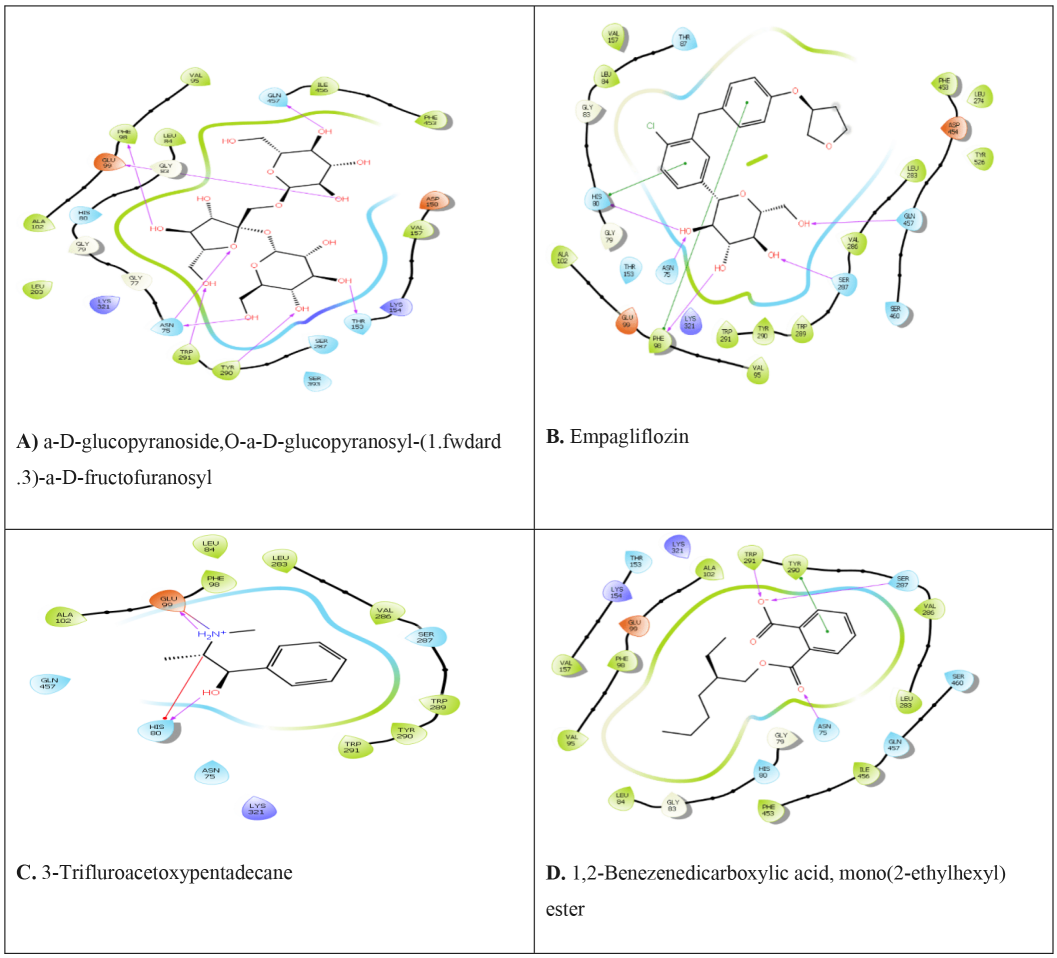
Table 2. Docking scores of constituents of *S. cordata* with diabetic proteins

S. No.	Name of the compound	Docking Score (7VSI)	Docking Score (4EMA)	Docking Score (7WMV)	Docking Score (1KAV)
1	1-2-Methylamine-1-phenyl propanol	-6.859	-5.112	-6.449	-4.063
2	2-Hexadecycloxycarbonyl-5-(2-hydroxyethyl)-4-methylimidazolium ion	-6.56	-7.47	-5.753	-1.242
3	Vitamin D_3	-6.1	-7.081	-5.889	-3.238
4	Spiro[androst-5ene-17,1-Cyclobutane]-2-one,3-hydroxy-, (3a,17a)-	-5.967	-3.336	-3.632	-2.164
5	Octadecanoic acid, ethyl ester	-5.588	-6.712	-6.044	-2.324
6	Cis-Z-a-Bisbolene epoxide	-4.815	-6.02	-4.889	-2.114
7	Diethylene glycol monododecyl ether	-4.521	-4.886	-5.368	-0.247
8	Z,Z-2,5-pentadecadien-1-ol	-3.957	-4.334	-4.095	-1.41
9	Octadecane, 1-(ethenyloxy)-	-1.865	-4.379	-4.345	-1.27
10	9,12,15-octadecatrienoic acid,2-[(trimethylsilyl)oxy]-1-[[trimethylsilyl) oxy]methyl] ethyl ester (Z,Z,Z)	0.294	-5.65	-5.968	-0.204
11	3-Trifluroacetoxypentadecane	-6.727	-7.313	-7.421	-0.497
12	2-piperidinone, N-[4-bromo-n-butyl]	-5.976	-7.951	-5.562	-2.909
13	2H-pyran,2-(7-heptadecynyloxy) tetrahydro-	-5.564	-7.191	-7.627	-1.157
14	[3R]-1,2,3,9-tetrahydropyrrolo [2,1-b] quinazolin-3-ol	-5.304	-2.471	-5.602	-0.002
15	Methoxy acetic acid, 4-tetradecyl ester	-4.257	-4.939	-4.728	-0.023
16	1,2-15,16-Diepoxyhexadecane	-3.642	-5.437	-4.914	-2.839
17	1-iodo-2-methylundecane	-3.407	-4.266	-3.143	-0.352
18	Squalene	-2.943	-3.298	-5.371	-2.213
19	Oleic acid	-2.739	-6.224	-4.853	-4.356
20	a-D-glucopyranoside,O-a-D-glucopyranosyl-(1.fwdard.3)-a-D-fructofuranosyl	-12.945	-11.231	-10.961	-7.522
21	1,2-Benezenedicarboxylic acid, mono(2-ethylhexyl) ester	-6.766	-7.998	-7.796	-3.173
22	3S-Hydroxy-2,3-dihydro-1H-pyrrolo [2,1-b] quinazolin-9-one	-5.442	-6.004	-6.601	-3.922
23	9,12-octadecadienoic acid, methyl ester, (E,E)	-5.201	-5.493	-5.694	-2.007
24	9,12,15-octadecadienoic acid,methyl ester, (Z,Z,Z)	-4.978	-6.682	-5.233	-1.426
25	1-Hexadecanol, 2-methyl-	-4.396	-4.779	-4.875	-3.853
26	Nonanoic acid	-4.383	-4.622	-4.065	-5.795
27	Dodecane, 2,6,10-Trimethyl-	-3.044	-4.017	-3.577	1.213
28	Vitamin E	-2.266	-6.232	-7.949	-2.518

by providing atom-level insights into molecular behavior. In this study, MD simulations were utilized to assess the conformational changes induced upon ligand binding to the target protein. Both the protein and the protein-ligand complex had a number of characteristics, including RMSD, RMSF, Rg, SASA, and inter-hydrogen bonding, determined. The complexes are 7VSI-APO, i.e. Protein alone, 7VSI-DRG is protein with a-D-glucopyranoside, and 7VSI-STD is protein with empagliflozin[19].

3.3.1 Root Mean Square Deviation (RMSD)

To assess the structural stability of the protein-ligand complexes and gain mechanistic insights into system dynamics, Root Mean Square Deviation (RMSD) values were calculated throughout a 100 ns molecular dynamics simulation, as depicted in Figure 5. All systems achieved equilibrium within the initial 10 ns and exhibited stable trajectories thereafter. The RMSD profiles of 7VSI-APO, 7VSI-DRG, and 7VSI-STD remained consistent over the simulation period, with mean RMSD values



A) a-D-glucopyranoside,O-a-D-glucopyranosyl-(1.fwdard .3)-a-D-fructofuranosyl

B. Empagliflozin

C. 3-Trifluroacetoxypentadecane

D. 1,2-Benezenedicarboxylic acid, mono(2-ethylhexyl) ester

E. 1-2-Methylamine-1-phenyl propanol

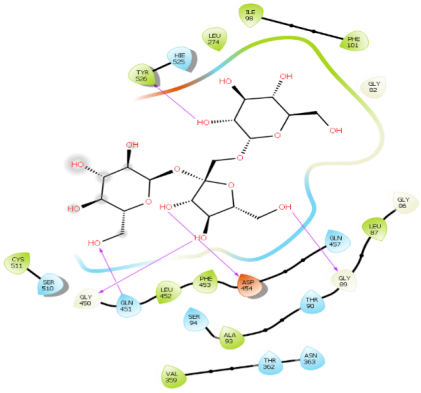
F. 2-Hexadecycloxycarbonyl-5-(2-hydroxyethyl)-4-methylimidazolium ion

Charged (negative)
Charged (positive)
Glycine
Hydrophobic
Metal
Polar
Unspecified residue
Water
Hydration site
Hydration site (displaced)
Distance
H-bond
Halogen bond
Metal coordination
Pi-Pi stacking
Pi-cation
Salt bridge
Solvent exposure

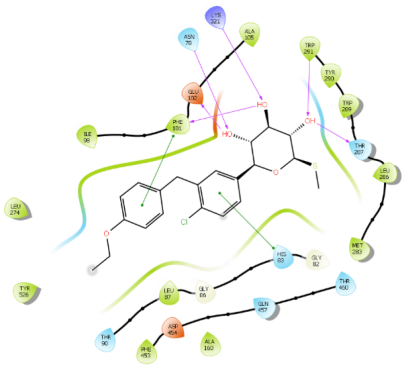
Figure 1 . 2D docking image of phyto-compounds of *S. cordata* with 7VSI.

Table 3. Docking score of most active phyto compound of *S. cordata* with 7VSI - Structure of human SGLT2-MAP17 complex bound with empagliflozin

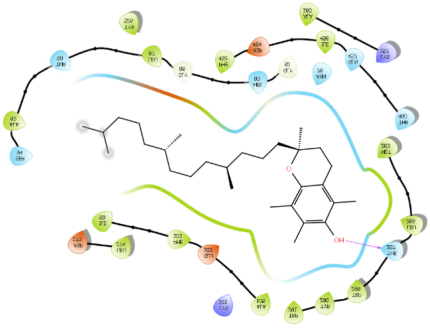
Compound name	Glide g score	Glide emode	H bond	Interaction residues
a-D-glucopyranoside,O-a-D-glucopyranosyl-(1.fwdard.3)-a-D-fructofuranosyl	-12.945	-63.196	-7.277	V157, LEV84, PHE453, LEV274, TYR526, LEV283, VAL286, TRP291, TYR290, TRP289, ALA102, PHE98, VAL95
Empagliflozin	-10.519	-110.322	------	VAL157, LEV84, ALA102, PHE98, VAL95, AL95, TRP291, TYP290, TRP289, VAL286, LEV283, PHE453, LEV274, TYR526
3-Trifluroacetoxypentadecane -6.727	-6.727	-56.639	-1.33	LEV84, ALA102, PHE98, PRP291, TRY290, TRP289, VAL286, LEV283
1,2-Benezenedicarboxylic acid, mono(2-ethylhexyl) ester	-6.766	-57.416	-1.39	ALA102, PHE98, VAL157, VAL95, LEV84, PHE453, ILE456, LEV283, VAL286, TYR290, TRP291
1-2-Methylamine-1-phenyl propanol	-6.866	-46.804	-2.23	ALA102, PHE98, VAL98, VAL95, TRY526, LEV274, TRP291, TRY290, TRO289, VAL286, LEV283, VAL157, PHE453, LEV84
2-Hexadecycloxycarbonyl-5-(2-hydroxyethyl)-4-methylimidazolium ion	-6.605	-77.125	-1.33	TRY526, LEV274, LEV84, PHE453, ILE456, VAL157, VAL359, ALA102, TRY290, TRP291, VAL95, LEV283



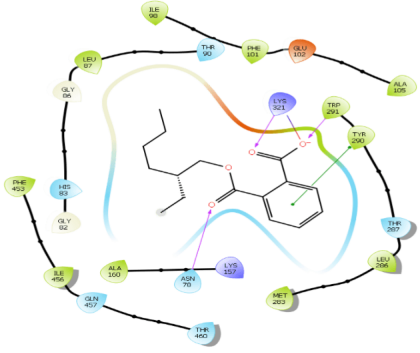
A. a-D-glucopyranoside,O-a-D-glucopyranosyl-(1.fwdard.3)-a-D-fructofuranosyl



B. LX2761



C. Vitamin E



D. 1,2-Benezenedicarboxylic acid, mono(2-ethylhexyl) ester

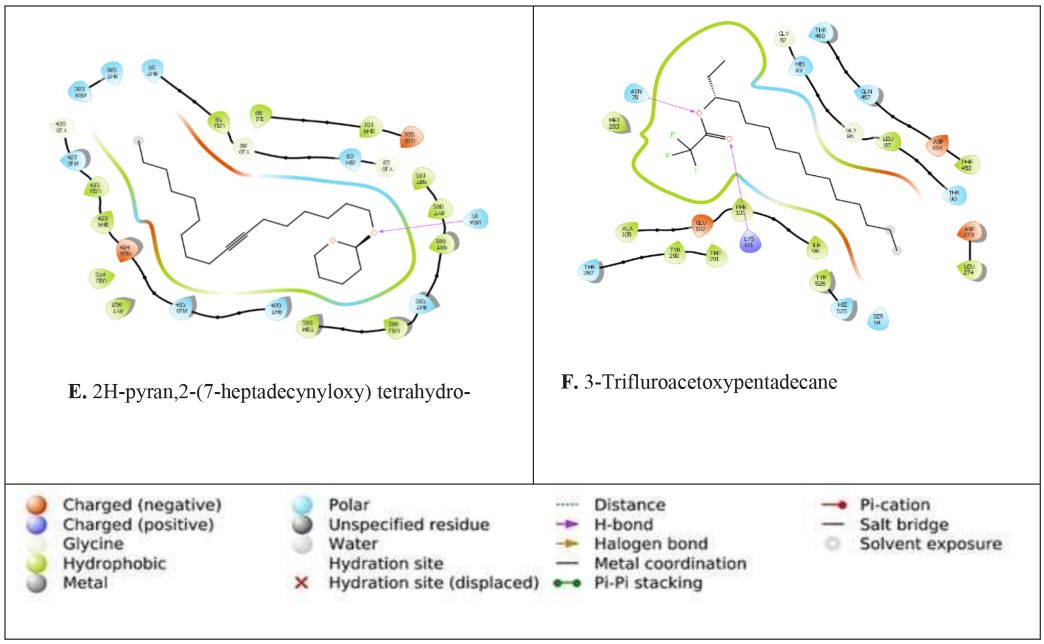


Figure 2. 2D docking image of phyto compound of *S. cordata* with 7WMV.

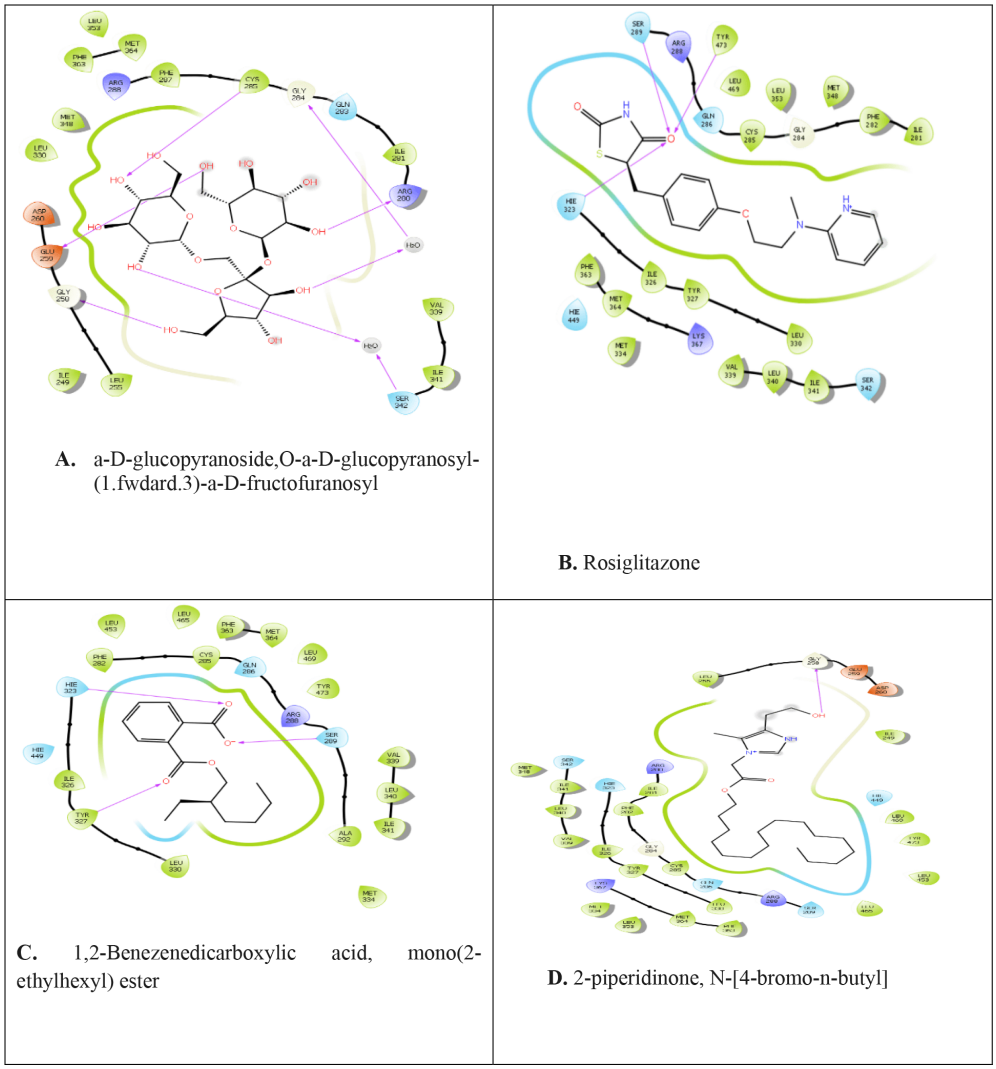
Table 4. Docking score of most active phyto compound of *S. cordata* with Structure of human SGLT1-MAP17 complex bound with LX2761

Compound name	Glide g score	Glide emode	H bond	Interaction residues
a-D-glucopyranoside,O-a-D-glucopyranosyl-(1.fwdard.3)-a-D-fructofuranosyl	-12.945	-63.196	-7.277	PHE101, ILE98, LEV274, TRY526, CYS511, LEV452, PHE453, ALA93, VAL359, LEV87
LX2761	-10.46	-96.596	-	ALA105, PHE101, ILE98, LEV274, PHE453, ALA160, MET23, LEV26, TRP289, TRY290, TRP291
Vitamin E -7.949	-7.949	-60.824	0	TRP29, TYR292, TRP291, ALA105, PHE101, LEV274, ILE98, ALA93, TRY526, LEV87, PHE453, ILE456, ALA160, MET283, LEV286
1,2-Benezenedicarboxylic acid, mono(2-ethylhexyl) ester	-7.796	-64.049	-1.197	PHE101, ILE98, ALA105, LEV87, PHE453, ILE456, ALA160, MET283, LEV286, TRY290, TRP29
2H-pyran,2-(7-heptadecynyloxy) tetrahydro-	-7.627	-55.852	0	TYR526, LEV274, PHE453, LEV452, LEV87, ILE98, PHE101, TRP291, TYR290, TYR289, LEV286, MET283
3-Trifluroacetoxypentadecane	-7.421	-54.125	0	MET283, ALA105, PHE101, ILE98, TRY290, TPR291, TRY526, LEV274, PHE453, LEV7

of 0.26 ± 0.02 nm, 0.25 ± 0.05 nm, and 0.25 ± 0.03 nm, respectively. These results demonstrate that the docked complexes, particularly 7VSI-DRG and 7VSI-STD, retained conformational stability without significant structural deviations, indicating reliable binding and overall system robustness.

3.3.2 Root Mean Square Fluctuation (RMSF)

Root mean square fluctuation (RMSF) analysis was performed to evaluate residue-level flexibility and identify conformational variations within protein regions during molecular dynamics simulations. RMSF provides insight into the dynamic behavior of individual residues and is particularly useful for assessing the influence of ligand binding on protein flexibility. Typically, elevated RMSF values correspond to disordered loop regions, while lower values are observed in more structured elements such as α-helices and β-sheets. In this study, RMSF values were calculated for each residue of the 7VSI-APO,



A. a-D-glucopyranoside,O-a-D-glucopyranosyl-(1.fwdard.3)-a-D-fructofuranosyl

B. Rosiglitazone

C. 1,2-Benezenedicarboxylic acid, mono(2-ethylhexyl) ester

D. 2-piperidinone, N-[4-bromo-n-butyl]

E. 2-Hexadecycloxycarbonyl-5-(2-hydroxyethyl)-4-methylimidazolium ion

F. Vitamin D_3

Charged (negative) · Charged (positive) · Glycine · Hydrophobic · Metal · Polar · Unspecified residue · Water · Hydration site · Hydration site (displaced) · Distance · H-bond · Halogen bond · Metal coordination · Pi-Pi stacking · Pi-cation · Salt bridge · Solvent exposure

Figure 3. 2D docking image of phyto compound of *S. cordata* with 4EMA.

Table 5. Docking score of most active phyto compound of *S. cordata* with structure of 4EMA- human peroxisome proliferator-activated receptor gamma in complex with

Compound name	Glide g score	Glide emode	H bond	Interaction residues
a-D-glucopyranoside,O-a-D-glucopyranosyl-(1.fwdard.3)-a-D-fructofuranosyl	-11.231	-62.931	-6.684	LEV353, PHE303, MET364, MET318, LEV320, PHE297, CYS285, ILE249,LEV255, ILE341, VAL339, ILE291.
Rosiglitazone	-10.46	-90.896	-	TYR473, LEV469, LEV353, MET348, PHE282, ILE281, CYS285, PHE363, MET364, VAL339, LEV340, ILE341,MET334, ILE326, TRY37, LEV330.
1,2-Benezenedicarboxylic acid, mono(2-ethylhexyl) ester -7.998	-7.998	-62.931	-0.655	LEV453, LEV465, PHE363, MET364, LEV469, TRY473, PHE282, CYS285, ALA292, ILE326, TRY327, LEV330, VAL339, LEV340, ILE341, MET334.
2-piperidinone, N-[4-bromo-n-butyl]	-7.951	-35.416	-1.004	LEV255, MET318, ILE341, LEV340, VAL339, ILE32, TRY327, MET334, LEV353, MET304, PHE353, LEV460, TYR473, LEV453, ILE465.
2-Hexadecycloxycarbonyl-5-(2-hydroxyethyl)-4-methylimidazolium ion	-7.47	-71.209	-0.301	MET348, ILE341, LEV340, VAL339, MET334, LEV353, ILE326, TRY327, LEV330, MET364, PHE363, LEV456, LEV453, TRY473, LEV459, ILE259, LEV255.
Vitamin D_3	-7.081	-37.078	0	TYR473, ALA292, LEV453, LEV469, LEV465, PHE363, MET364, MET346, ILE281, PHE282, CYS285, MET334, LEV333, LEV330, TRY327, ILE341, LEV340, VAL339.

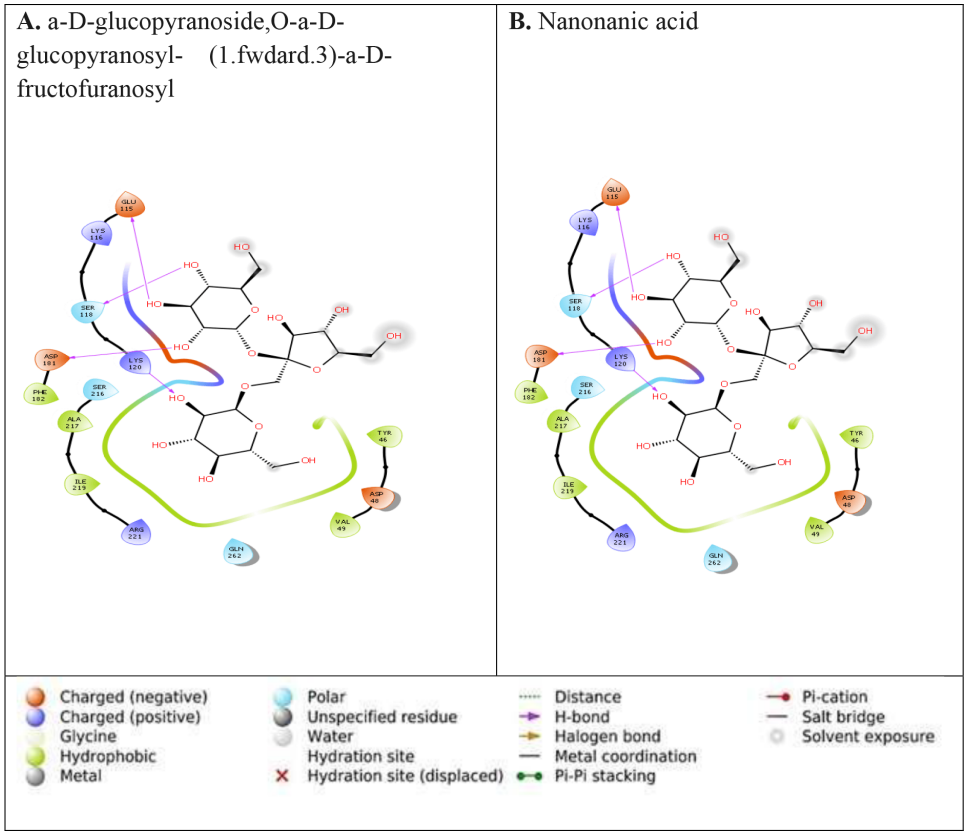


Figure 4. 2D docking image of phyto compound of *S. cordata* with 1KAV.

Table 6. Docking score of most active phyto compound of *S. cordata* with structure of 1KAV - Human Tyrosine Phosphatase 1B Complexed with an Inhibitor

Compound name	Glide g score	Glide emode	H bond	Interaction residues
a-D-glucopyranoside,O-a-D-glucopyranosyl-(1. fwdard.3)-a-D-fructofuranosyl -7.552	-7.552	-40.227	-4.867	PHE182, ALA217, ILE219 VAL49, TYR46.
Nanonanic acid	-5.795	-46.547	-3.419	PHE182, ILE219, ALA217, CYS215, VAL49, TRY46

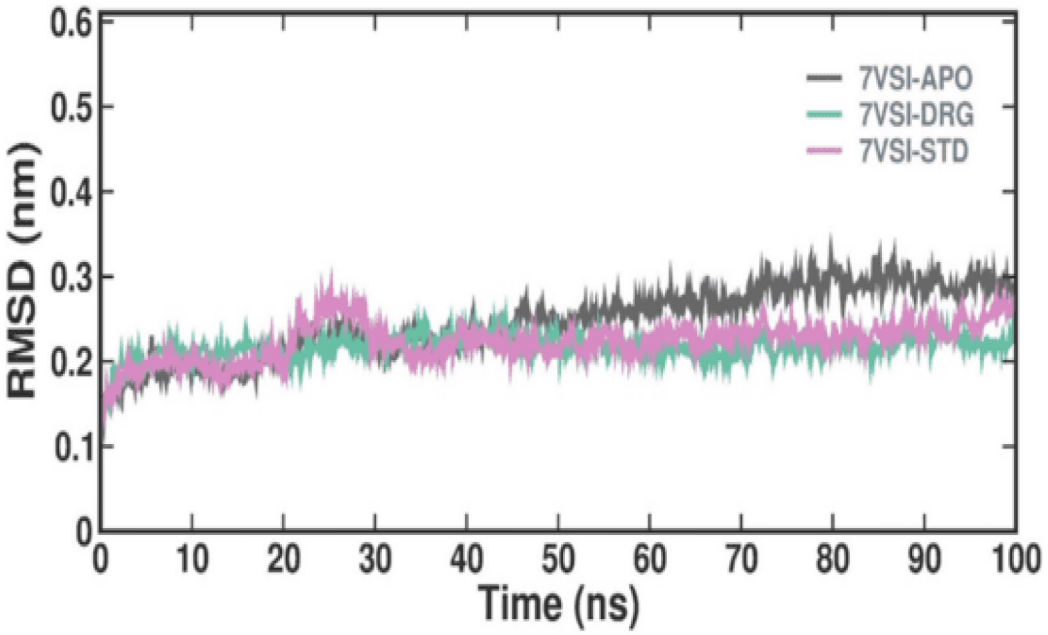


Figure 5. RMSD conformational dynamics analysis of 7VSI-DRG and 7VSI-STD.

7VSI-DRG, and 7VSI-STD complexes, as illustrated in Figure 6. The average RMSF values for 7VSI-APO, 7VSI-DRG, and 7VSI-STD were 0.16 ± 0.09 nm, 0.15 ± 0.06 nm, and 0.16 ± 0.09 nm, respectively. These findings suggest that ligand binding in the 7VSI-DRG and 7VSI-STD complexes did not induce notable changes in residue flexibility when compared to the unbound protein.

3.3.3 Radius of Gyration (RG)

To evaluate the conformational stability and tertiary structure integrity of the 7VSI-DRG and 7VSI-STD complexes, the radius of gyration (RG) was computed and plotted across the simulation timeframe (Figure 7). The average RG values for 7VSI-APO, 7VSI-DRG, and 7VSI-STD were 2.41 ± 0.04 nm, 2.47 ± 0.02 nm, and 2.45 ± 0.01 nm, respectively. The Rg profiles of both 7VSI-DRG and 7VSI-STD exhibited minimal fluctuations, indicating preservation of tertiary structure and consistent molecular packing throughout the simulation. These results suggest that ligand binding did not induce significant destabilization of the protein's overall structure.

3.3.4 Solvent Accessible Surface Area (SASA)

During the molecular modelling process, SASA values were computed and analysed to investigate the effect of 7VSI-STD binding on the solvent exposure of the target protein (Figure 8). The resulting SASA profiles of 7VSI-DRG and 7VSI-STD displayed similar trends, indicating comparable solvent accessibility. The average SASA values for 7VSI-APO, 7VSI-DRG, and 7VSI-STD were 268.42 ± 3.6 nm^2, 265.87 ± 3.2 nm^2, and 266.39 ± 3.005 nm^2, respectively. These values exhibited stable equilibration with no substantial fluctuations, suggesting that ligand binding did not markedly alter the protein's solvent-exposed surface during the molecular modelling process.

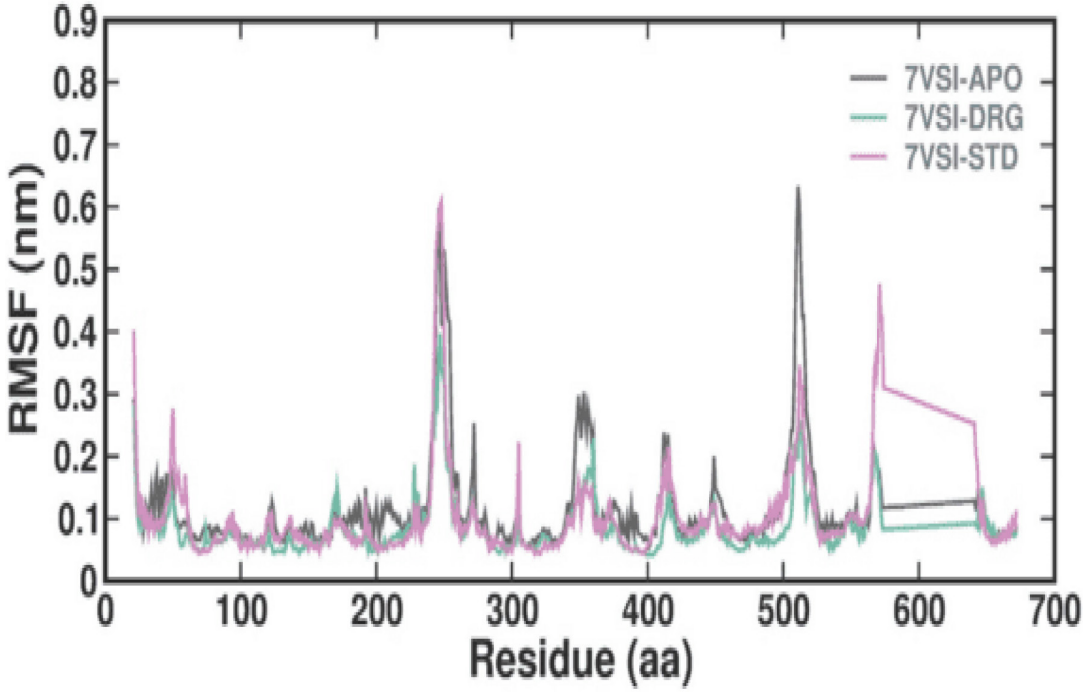


Figure 6. RMSF conformational dynamics analysis of 7VSI-APO, 7VSI-DRG and 7VSI-STD complex.

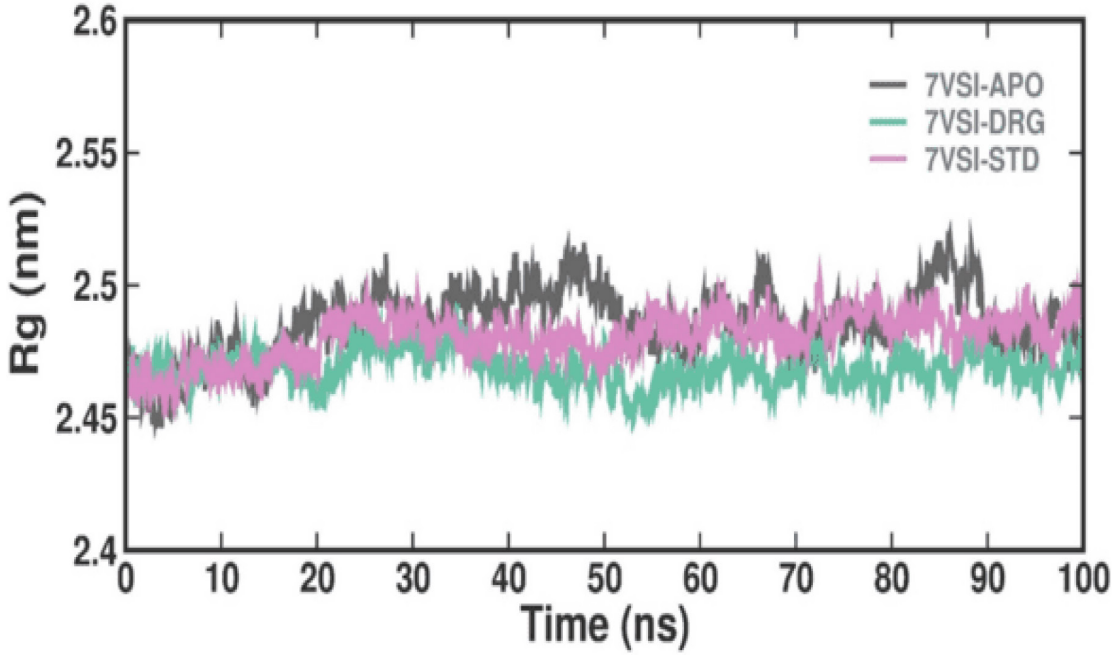


Figure 7. Rg conformational dynamics analysis of 7VSI-APO, 7VSI-DRG and 7VSI-STD complex.

3.2.5 Intra and Inter Hydrogen Bond

To evaluate the structural stability of the unbound protein (7VSI-APO) and protein-ligand complexes (7VSI-DRG and 7VSI-STD), the formation of intra- and intermolecular hydrogen bonds was analysed, given their key role in maintaining conformational integrity and ligand binding. The time-resolved behaviour of intramolecular hydrogen bonds was assessed throughout the molecular modelling process, and the results were plotted accordingly (Figure 9).

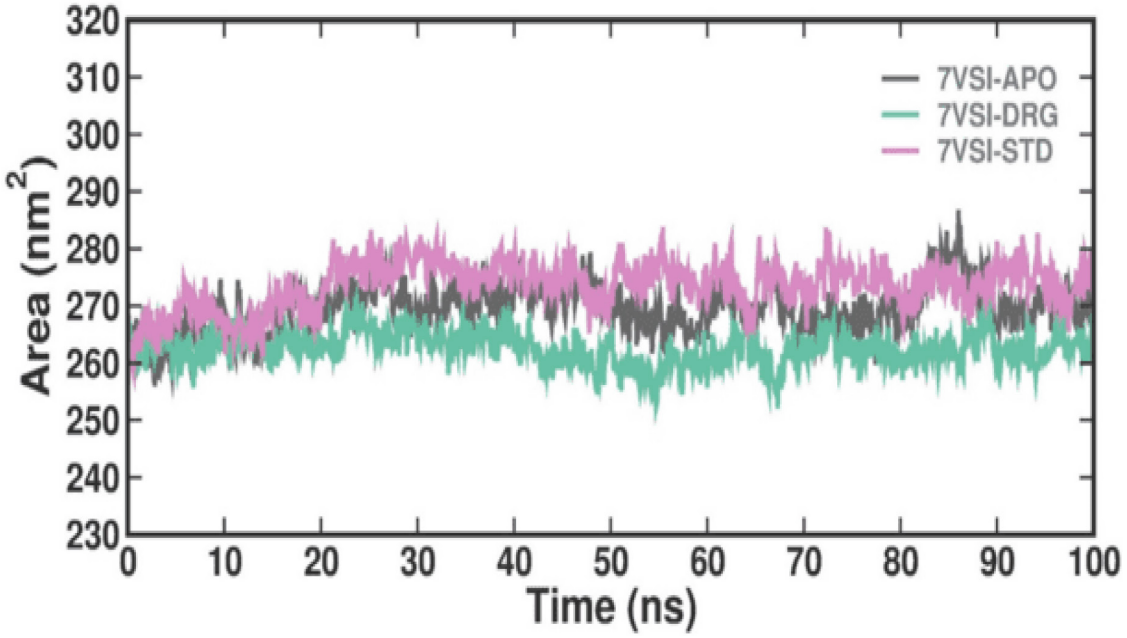


Figure 8. SASA conformational dynamics analysis of 7VSI-APO, 7VSI-DRG and 7VSI-STD complex.

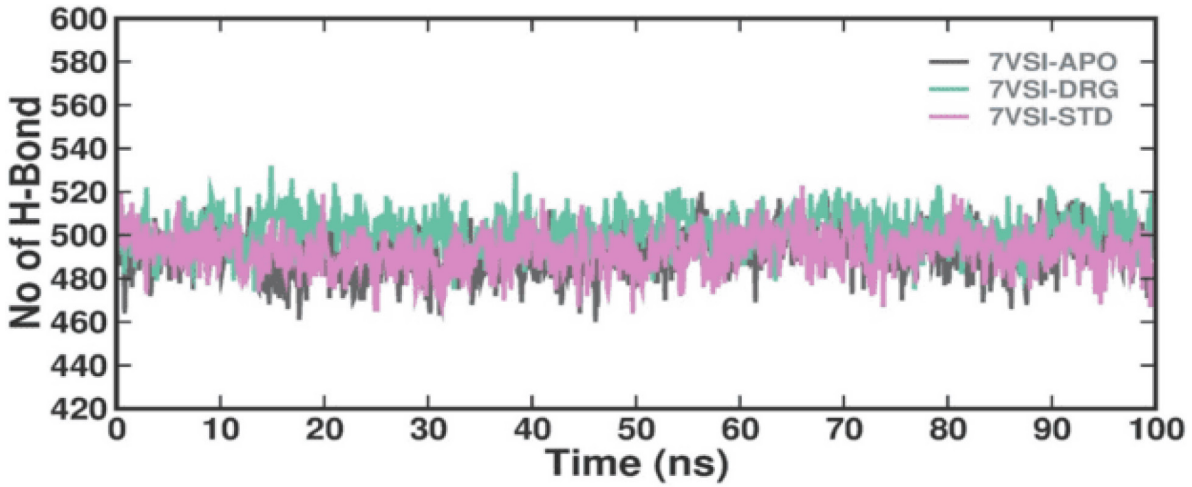


Figure 9. Intra molecular hydrogen bonds 7VSI-APO and 7VSI-DRG and 7VSI-STD during the simulation time.

The average number of intramolecular hydrogen bonds observed for 7VSI-APO, 7VSI-DRG, and 7VSI-STD was 551.92 ± 7.8, 549.54 ± 8.09, and 548.19 ± 8.3, respectively. Although the apo form displayed slightly higher hydrogen bond counts, the profiles of the ligand-bound complexes demonstrated consistent hydrogen bonding, indicating stable folded conformations upon ligand interaction.

To further assess the protein-ligand binding stability, the number of intermolecular hydrogen bonds between the protein and ligands was monitored over time (Figure 10). The 7VSI-DRG complex maintained between 1 and 4 hydrogen bonds, while the 7VSI-STD complex exhibited a range of 1 to 10 hydrogen bonds throughout the simulation. These interactions suggest that the docked ligands contributed to stable and sustained binding with the target protein over the simulation period.

3.3.6 Principal Component Analysis (PCA)

To investigate the collective atomic motions and conformational dynamics of the 7VSI-APO, 7VSI-DRG,

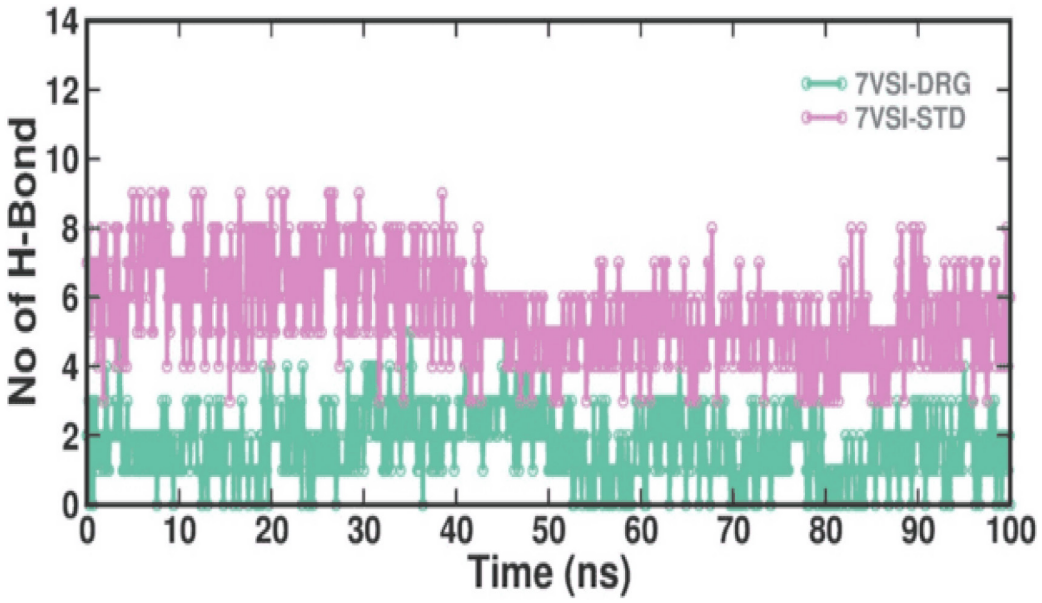


Figure 10. Intermolecular hydrogen bonds between protein-ligand during the simulation time.

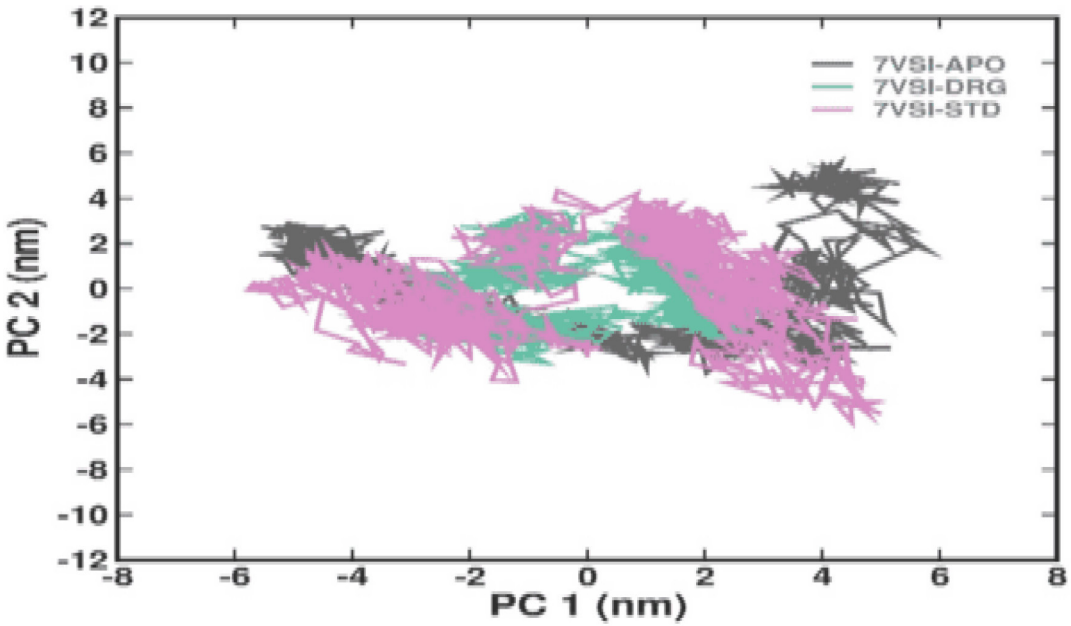


Figure 11. Principal component analysis 2D projection plot shows the conformation sampling of 7VSI-APO and 7VSI-DRG and 7VSI-STD on PC1 and PC2.

and 7VSI-STD systems, Principal Component Analysis (PCA) was performed. The initial principal eigenvectors (EVs) typically capture the dominant global motions within protein structures. Accordingly, PCA was employed to analyse the dynamic behaviour of these complexes throughout the simulation trajectory. The temporal evolution of the principal components revealed reduced amplitude in the collective motions for all systems, particularly in 7VSI-DRG and 7VSI-STD, indicating enhanced structural stability (Figure 11). The PCA projections showed substantial overlap in the conformational space occupied by the apo and ligand-bound forms, suggesting that ligand binding did not induce significant conformational shifts. Overall, the lower degree of motion observed in 7VSI-DRG and 7VSI-STD complexes reinforces the notion of

conformational restraint and structural stability upon ligand association.

3.3.7 MM - PBSA

To gain deeper insight into the binding affinities of the 7VSI-DRG and 7VSI-STD complexes, we assessed their interaction strengths through a comprehensive energy analysis (Table 7) presents a comparative overview of the binding free energies for both inhibitors, calculated using the Molecular Mechanics Poisson–Boltzmann Surface Area (MM-PBSA) approach. Energy values were derived from equilibrated frames of the simulation trajectory, enabling a detailed residue-level decomposition to elucidate the specific contributions governing ligand–protein interactions.

4. ADMET and Drug-likeness Evaluation

The ADMET and drug-likeness properties of the selected lead compounds were predicted using the SwissADME tool to evaluate their pharmacokinetic behavior and safety profile. The lead compound, α-D-glucopyranoside, exhibited an acceptable molecular weight (504.4 g/mol) with only one Lipinski rule

Table 7. Binding free energy for 7VSI complexes with standard and a-D-glucopyranoside bound complexes

Binding free energy values of complex	van der Waal energy (kj/mol)	Electrostatic energy (kj/mol)	Polar solvation energy (kj/mol)	Binding energy (kj/mol)
7VSI-DRG	-140.303+/-18.884	-115.181 +/- 14.836	189.960 +/- 13.892	-82.547 +/-15.257
7VSI-STD	-151.027+/- 9.047	-11.816 +/- 6.595	77.143 +/- 12.490	-102.457 +/- 9.064

Table 8. Predicted ADMET properties (SwissADME)

Parameter	α-D-glucopyranoside	Vitamin E	Oleic acid	Squalene
Molecular Weight (g/mol)	504.4	430.7	282.5	410.7
Lipinski Rule Violation	1	1	0	1
GI Absorption	Moderate	High	High	Low
BBB Permeability	No	Yes	No	No
Bioavailability Score	0.55	0.55	0.85	0.17
Toxicity Alerts	None	None	None	None

Table 9. ADMET and drug-likeness profile of selected phytoconstituents

ADMET Parameter	α-D-glucopyranoside	Vitamin E	Oleic Acid	Squalene
Molecular Weight (g/mol)	504.4	430.7	282.5	410.7
Hydrogen Bond Donors	8	1	1	0
Hydrogen Bond Acceptors	11	2	2	0
Lipinski Rule Violations	1	1	0	1
GI Absorption	Moderate	High	High	Low
BBB Permeability	No	Yes	No	No
P-gp Substrate	Yes	No	No	No
CYP Inhibition	None	None	None	None
Bioavailability Score	0.55	0.55	0.85	0.17
Hepatotoxicity	No	No	No	No
Mutagenicity	No	No	No	No
Cardiotoxicity (hERG)	No	No	No	No
Drug-Likeness	Acceptable	Acceptable	High	Moderate

violation, which is commonly observed for glycoside molecules. It showed moderate gastrointestinal absorption and a bioavailability score of 0.55, indicating reasonable oral availability (Table 8). Importantly, the compound was predicted to be non-toxic and unable to cross the blood–brain barrier, which is favorable for antidiabetic agents as it minimizes central nervous system side effects. Comparative compounds such as vitamin E and oleic acid showed higher GI absorption but lacked strong target-specific interactions, while squalene exhibited poor bioavailability. (Table 9) Overall, the ADMET analysis supports that α-D-glucopyranoside possesses a balanced pharmacokinetic profile with good safety characteristics, reinforcing its potential as a promising antidiabetic lead molecule.

5. Discussion

Diabetes mellitus is a chronic metabolic disorder characterised by persistent hyperglycaemia resulting from impaired insulin secretion and insulin action[20]. The present discussion focuses on the molecular-level interactions of *S. cordata* phytoconstituents with diabetes-associated protein targets, as revealed through *in silico* approaches. Plants and plant extracts are vital in modern medicine due to their rich chemical and therapeutic properties. Many existing drugs are derived from plant sources, and *Sida* species ("*Bala*") are known to exhibit analgesic, anti-inflammatory, hypoglycemic, and hepatoprotective activities[21]. *S. cordata* contains diverse bioactive constituents, including primary metabolites, sugars, amino acids, proteins and pharmacologically important secondary metabolites such as alkaloids, flavonoids, and tannins[22]. CCl_4 elevated serum liver enzymes, while *S. cordata* ethanolic extract reversed this effect and significantly enhanced hepatic antioxidant enzymes, indicating strong hepatoprotective activity[23]. cytotoxic activities and protected kidneys from CCl_4 damage, and improved diabetes via glucose and oxidative stress regulation[24]. Phyto-components of *S. cordata* were docked with proteins, such as the structure of human SGLT2-MAP17 complex bound with empagliflozin, the structure of human SGLT1-MAP17 complex bound with LX2761, Human peroxisome proliferator-activated receptor gamma in complex with rosiglitazone, Human Tyrosine Phosphatase 1B Complexed with an inhibitor using computational methods such as molecular docking and dynamics. Docking analysis was performed between ligands and the target protein 7VSI, 7WMV, 4EMA, 1KAV. The docking program assessed the ligand and protein docking using a related scoring function, where a greater negative value indicated better docking. The program's scoring feature, known as the G-score, reveals a ligand's ability to bind to a specific protein receptor shape. The target scoring function, expected even in the lowest energy pose, is used to evaluate the accuracy of the docking method (binding conformation) [25]. In this investigation, the binding energy, H-bonds, and G-score were used to assess the effectiveness of the docking process by removing the inhibitor molecule from the proteins. Efficient docking has been linked to both lipophilic contacts between the ligand and the receptor and strong intermolecular hydrogen bonding, according to the entire set of results. With a range of -1.4 to -12.9, all the drugs have shown moderate to strong inhibition. α-D-glucopyranoside has demonstrated strong inhibition with docking scores of -12.9, -11.231, -10.961, and -7.522 with 7VSI, 4EMA, 7WMV, and 1KAV, in that order. A larger negative value denotes a stronger docking score. These derivatives are anticipated to show good antidiabetic properties with minimal adverse effects because the developed analogues exhibited strong binding affinities and formed favourable interactions within the active site of the target protein. α-D-glucopyranoside showed the higher binding affinity of -12.9 with 7VSI - Structure of human SGLT2-MAP17 complex bound with empagliflozin. Detailed interaction analysis revealed that this compound formed stable hydrogen bonds and hydrophobic interactions with key amino acid residues, including CYS285, TYR473, MET364, LEU353, ILE341, and VAL339, which are known to play critical roles in enzymatic activity and ligand stabilization The dominance of hydrophobic residues in the binding sites further explains why glycoside compounds with balanced polar and non-polar features exhibited superior binding compared to long-chain fatty acids and hydrocarbons. The observed binding pattern aligns with reported mechanisms of α-glucosidase inhibition, providing a molecular basis for the traditional antidiabetic use of *S. cordata*. Overall, the results highlight α-D-glucopyranoside derivatives as promising lead molecules for further experimental

validation. The top-ranked ligand complexes obtained from molecular docking studies, specifically 7VSI-DRG and 7VSI-STD, were selected for molecular dynamics simulations. The ligand topologies were generated using the Automated Topology Builder (ATB) server. Hydrogen atoms were added to heavy atoms using the pdb2gmx module in the GROMACS simulation suite. The prepared systems underwent energy minimisation under vacuum conditions for 1500 steps, utilising the steepest descent algorithm to relieve any steric clashes[26]. Post-minimization, the systems were solvated within a cubic periodic boundary box employing the Simple Point Charge Extended (SPC/E) water model. To emulate physiological ionic strength, counterions (Na^+ and Cl^-) were introduced to achieve an overall salt concentration of 0.15 M. Afterwards, each system underwent equilibration under constant pressure and temperature (NPT ensemble), followed by a production MD simulation run of 200 nanoseconds. Simulation trajectories were analysed using standard GROMACS utilities to evaluate structural and dynamic properties, including RMSD, RMSF, radius of gyration (Rg), Solvent- Accessible Surface Area (SASA), and hydrogen bond interactions.

Additionally, the Molecular Mechanics Poisson–Boltzmann Surface Area (MM-PBSA) method was employed to calculate the binding free energy of 7VSI-DRG and 7VSI-STD with the target protein across the simulation time frame. RMSD values 7VSI-DRG and 7VSI-STD were 0.25 +/- 0.05 nm and 0.25 +/- 0.03 nm, respectively, which indicates a stable system that did not exhibit fluctuations. The average RMSF values for 7VSI-DRG were found to be 0.15 +/- 0.06 nm, and the complex did not significantly alter the overall RMSF distribution. According to the results, the complex system of 7VSI-DRG exhibited almost similar Rg values as compared to the 7VSI-STD, which leads to similar compactness of both complex systems. The SASA values of complex 7VSI-DRG were 265.87 +/- 3.2 nm, which showed fair equilibration. The Intra H-Bond values for 7VSI-APO and 7VSI-DRG, and 7VSI-STD complex were found to be 551.92 +/- 7.8 nm, 549.54 +/- 8.09 nm and 548.19 +/- 8.3 nm, respectively and compared to the 7VSI-APO structure, both 7VSI-DRG and 7VSI-STD complexes demonstrated superior stability throughout the simulation. The collective moments of the complex did not affect the target conformation and dynamics, which showed the stability. The MM-PBSA analysis showed the binding strength or free energy was more stable for the 7VSI-DRG complex. The parameters of molecular dynamics showed stability of α-D-glucopyranoside with the structure of human SGLT2-MAP17 complex bound with Empagliflozin complex[27]. The results of molecular docking simulations showed that α-D-glucopyranoside had greater binding scores and strong nonbonding interactions with 4URO and 4XE3 compared to the original molecules. Through molecular dynamics simulations lasting 2500 picoseconds, it was verified that the protein-ligand combination remains stable in biological systems. The α-D-glucopyranoside derivative from *S. cordata* exhibits antidiabetic potential through a multi-target inhibitory mechanism. Although α-D-glucopyranoside derivatives are widely reported to exert antidiabetic effects primarily via α-glucosidase inhibition. These findings suggest that the α-D-glucopyranoside derivative may modulate glucose metabolism through simultaneous inhibition of multiple diabetic pathways, rather than acting solely through α-glucosidase inhibition, thereby providing a mechanistic basis for the traditional antidiabetic use of *S. cordata*[28]. The molecular docking analysis indicates that the investigated drugs demonstrate robust binding affinities and display notable efficacy against bacteria and fungi. More precisely, α-D-glucopyranoside exhibits the greatest docking score against COVID-19[29]. The introduction of methyl α-D-glucopyranoside (α-MG) enhanced the specific activity and relaxed. The formation and structural arrangement of recombinant β-galactosidase inclusion bodies in *E. coli*, induced through the araBAD promoter system, were investigated[30]. *In silico* ADMET screening is a critical step in early-stage drug discovery, as it helps to eliminate compounds with poor absorption or toxicity before experimental validation. The lead compound, α-D-glucopyranoside derivative, demonstrated acceptable molecular weight, moderate gastrointestinal absorption, and favorable bioavailability, with no predicted toxicity alerts, indicating good oral drug-likeness. The results of molecular docking and dynamics studies, ADMET revealed that the α-D-glucopyranoside showed anti-diabetic activity. Computational methods have shown to be effective instruments and have achieved significant results in the field of computer-based studies. Based on the preceding discussion, it can be inferred that α-D-glucopyranoside can significantly advance the

pharmaceutical industry's research and development of anti-diabetic drugs[31].

6. Conclusion

Appropriate screening techniques could be employed to reduce both time and expenses throughout the drug discovery process. In this work, the binding ability between phyto-components has been analyzed using one of the efficient techniques, molecular docking with 7VSI, 7WMV, 4EMA, and 1KAV. α-D-glucopyranoside showed potent inhibition with a docking score of -12.9, also bound with active sites in a good manner. The binding affinity was due to polar interactions, mainly by hydrogen bonding. The molecular dynamics showed that the complex of α-D-glucopyranoside with the protein was more stable and might be a potential candidate for an antidiabetic agent. Further *in vitro* and *in vivo* studies need to be done for the α-D-glucopyranoside to explore the molecular mechanism for diabetes mellitus.

7. Acknowledgement

The authors thank the management of Sriramachandra Institute of Higher Education and Research (DU), Chennai, India, for their constant support and encouragement.

8. References

1. Alam S, Sarker MMR, Sultana TN, *et al.* Antidiabetic phytochemicals from medicinal plants: prospective candidates for new drug discovery and development. Front Endocrinol (Lausanne); 13. Epub ahead of print. 2022. https://doi.org/10.3389/fendo.2022.800714
2. Malviya N, Jain S, Malviya S. Antidiabetic potential of medicinal plants. Acta Pol Pharm - Drug Res. 2010; 67:113-118.
3. Yang W, Dall TM, Tan E, *et al.* Diabetes diagnosis and management among insured adults across metropolitan areas in the U.S. Prev Med Reports. 2018; 10:227-233. https://doi.org/10.1016/j.pmedr.2018.03.014
4. Reddy UC, Elizabeth H, Kiran RY. *In vitro* hepatoprotective activity of a selected siddha medicinal plant *Sida cordata*, using Chang liver cells. *In vitro* hepatoprotective acts against CCl4 induce toxicity in some siddha med plants. Pharmtech Res. 2012; 2. http://www.ajptr.com/
5. Rao VS, Srinivas K. Modern drug discovery process: An *in-silico* approach. J Bioinforma Seq Anal. 2011; 2:89-94.
6. Miyachi H. Structural biology inspired development of a series of human peroxisome proliferator-activated receptor gamma (PPARγ) ligands: from agonist to antagonist. Int J Mol Sci. Epub ahead of print. 2023; 24. https://doi.org/10.3390/ijms24043940
7. Encinar JA, Fernández-Ballester G, Galiano-Ibarra V, *et al. In silico* approach for the discovery of new PPARγ modulators among plant-derived polyphenols. Drug Des Devel Ther. 2015; 9:5877-5895. https://doi.org/10.2147/DDDT.S93449
8. Kuswandi A, Rusdin A, Tarawan VM, *et al.* Molecular docking study of the major compounds from *Garcinia atroviridis* on human SGLT-2 protein transport using structure-based drug design method. Int J Appl Pharm. 2022; 14:138-143. https://doi.org/10.22159/ijap.2022v14i4.44390
9. Akinnusi PA, Olubode SO, Alade AA, *et al.* Potential inhibitory biomolecular interactions of natural compounds with different molecular targets of diabetes. Bioinform Biol Insights; Epub ahead of print. 2023; 17. https://doi.org/10.1177/11779322231167970
10. Halgren TA. Identifying and characterising binding sites and assessing druggability. J Chem Inf Model 2009; 49:377-389. https://doi.org/10.1021/ci800324m
11. Singh S, Bani Baker Q, Singh DB. Molecular docking and molecular dynamics simulation. Bioinforma Methods Appl. 2021. pp.291-304. https://doi.org/10.1016/B978-0-323-89775-4.00014-6
12. Naveen YP, Urooj A, Byrappa K. A review on medicinal plants evaluated for anti-diabetic potential in clinical trials: Present status and future perspective. J Herb Med. 2021; 28:100436. https://doi.org/10.1016/j.hermed.2021.100436
13. Riyaphan J, Pham DC, Leong MK, *et al. In silico* approaches to identify polyphenol compounds as α-glucosidase and α-amylase inhibitors against type-ii diabetes. Biomolecules; 11. Epub ahead of print. 2021. https://doi.org/10.3390/biom11121877
14. Gupta RC, Chang D, Nammi S, *et al.* Interactions between antidiabetic drugs and herbs: An overview of mechanisms of action and clinical implications. Diabetol Metab Syndr. 2017; 9:1-12. https://doi.org/10.1186/s13098-017-0254-9
15. Ganesh M, Mohankumar M. Extraction and identification of bioactive components in *Sida cordata* (Burm.f.) using gas chromatography-mass spectrometry. J Food Sci Technol. 2017; 54:3082-3091. https://doi.org/10.1007/s13197-017-2744-z
16. Elampulakkadu A, Pathrose Thankamma M, Thirumoorthy P. *In Silico* design and molecular docking studies of benzimidazole-bearing thiazolidin-4-one derivatives as PPARγ agonists in diabetes mellitus. Int J Pharm Sci Rev Res. 2020; 65:88-91. https://doi.org/10.47583/ijpsrr.2020.v65i01.012

17. Rai H, Barik A, Singh YP, *et al.* Molecular docking, binding mode analysis, molecular dynamics, and prediction of ADMET/toxicity properties of selective potential antiviral agents against SARS-CoV-2 main protease: an effort toward drug repurposing to combat COVID-19. Mol Divers. 2021; 25:1905-1927. https://doi.org/10.1007/s11030-021-10188-5
18. Karodi R, Jadhav M, Rub R, *et al.* Evaluation of the wound healing activity of a crude extract of *Rubia cordifolia* L. (Indian madder) in mice. Int J Appl Res Nat Prod. 2009; 2:12-18.
19. Ravikumar Y, Koonyosying P, Srichairatanakool S, *et al. In silico* molecular docking and dynamics simulation analysis of potential histone lysine methyl transferase inhibitors for managing β-thalassemia. Molecules. 2023; 28. https://doi.org/10.3390/molecules28217266
20. Shah NA, Khan MR, Ahmad B, *et al.* Investigation on flavonoid composition and anti-free radical potential of *Sida cordata*. BMC Complement Altern Med. 2013; 13. https://doi.org/10.1186/1472-6882-13-276
21. Banni M, Jayaraj M. Profile of bioactive compounds, *in vitro* anticancerous and antioxidant activity of stem extracts of *Sida cordata*. Plant Biosyst. 2023; 157:1221-1233. https://doi.org/10.1080/11263504.2023.2260820
22. Shah NA, Khan MR, Nigussie D. Phytochemical investigation and nephroprotective potential of *Sida cordata* in rats. BMC Complement Altern Med. 2017; 17. https://doi.org/10.1186/s12906-017-1896-8
23. Mitra S, Anjum J, Muni M, *et al.* Exploring the journey of emodin as a potential neuroprotective agent: novel therapeutic insights with molecular mechanism of action. Biomedicine and Pharmacotherapy. 2022; 149. https://doi.org/10.1016/j.biopha.2022.112877
24. Gulnaz AR, Savitha G, *et al*. Evaluation of antimicrobial activity of leaf and stem extracts of *Siddha* medicinal plant *Sida cordata*. J Evol Med Dent Sci. 2013; 2(49):9573–9582.
25. Gnanaraj C, Sekar M, Fuloria S, *et al. In silico* molecular docking analysis of karanjin against alzheimer's and parkinson's diseases as a potential natural lead molecule for new drug design, development and therapy. Molecules. 2022; 27. https://doi.org/10.3390/molecules27092834
26. Le J, Chen Y, Yang W, *et al.* Metabolic basis of solute carrier transporters in the treatment of type 2 diabetes mellitus. Acta Pharm Sin B. 2024; 14:437-454. https://doi.org/10.1016/j.apsb.2023.09.004
27. Kayes MR, Saha S, Alanazi MM, *et al.* Macromolecules: synthesis, antimicrobial, POM analysis and computational approaches of some glucoside derivatives bearing acyl moieties. Saudi Pharm J. 2023; 31:101804. https://doi.org/10.1016/j.jsps.2023.101804
28. Kawsar SMA, Kumer A. Computational investigation of methyl α-d-glucopyranoside derivatives as inhibitors against bacteria, fungi and COVID-19 (sars-2). J Chil Chem Soc. 2021; 66:5206-5214. https://doi.org/10.4067/S0717-97072021000205206
29. Jung KH, Yeon JH, Moon SK, *et al.* Methyl α-D-glucopyranoside enhances the enzymatic activity of recombinant β-galactosidase inclusion bodies in the araBAD promoter system of *Escherichia coli*. J Ind Microbiol Biotechnol. 2008; 35:695-701. https://doi.org/10.1007/s10295-008-0329-6
30. Jang JY, Bae H, Lee YJ, *et al.* Structural basis for the enhanced anti-diabetic efficacy of lobeglitazone on PPARγ. Sci Rep. 2018; 8:1-11. https://doi.org/10.1038/s41598-017-18274-1
31. Kumar M, Mani S, Punnoose A, Ethayaraja M, *et al.* Plant description, phytochemical constituents and pharmacological attributes of the plant *Sida cordata*: a perspective review. 2025. https://doi.org/10.18311/jnr/2025/41920

Author Contribution

Dr Sangeetha Mani conceptualised the review and guided the research framework. Mahesh Kumar conducted the literature search, did the molecular docking, dynamics stimulation studies and analysed them. And drafted the manuscript. Dr Ethayaraja Mani contributed to manuscript editing, supervision, and final revisions. All authors read and approved the final manuscript. Dr Alan M. Punnoose Proofread and analysed the paper. All authors have read and agreed to the published version of the manuscript.